Complexity and Criticality in Neuro-Inspired Reservoirs

Michiel van der Vlag^{1,3⊠}₀, Alper Yegenoglu¹₀, Cristian Jimenez-Romero⁴₀, Abigail Morrison^{1,2,3}₀, and Sandra Diaz¹₀

¹ SDL Neuroscience, Forschungszentrum Jülich GmbH, Institute for Advanced Simulation, Jülich Supercomputing Centre (JSC), 52428 Jülich, Germany.

³ Department of Computer Science 3 - Software Engineering, RWTH Aachen University, Aachen, Germany morrison@fz-juelich.de

⁴ ETIS Lab, ENSEA, CNRS, UMR8051, CY Cergy-Paris University, Cergy, France. cristian.jimenez-romero@cyu.fr

Abstract. Understanding information propagation and computational capabilities in large-scale brain models is crucial for advancing both neuroscience and neuro-inspired computing. It remains unknown how complexity affects the performance of simulated biological networks in predicting non-linear dynamics. Here, this issue is addressed by integrating reservoir computing, a recurrent neural network architecture, with The Virtual Brain, a whole-brain simulation platform, to create a more neurophysiologically-plausible machine learning framework. Metrics derived from nonlinear dynamics and complexity theory, including the largest Lyapunov exponent, which captures chaotic behavior, Detrended Fluctuation Analysis, which assesses temporal correlations, and the Perturbational Complexity Index, which evaluates the complexity of neural responses, provide a quantitative framework for characterizing cognitive dynamics. Deploying this framework on High Performance Computing enables a thorough exploration of the vast parameter space, utilizing a diverse evaluation framework that assesses simulations through these metrics, implemented on Graphics Processing Units (GPUs). This enables the identification of optimal parameter regimes, a comprehensive characterization of the complex dynamics exhibited by the system, and a deeper understanding of the underlying mechanisms governing the TVB-based reservoir's computational capabilities. Ridge regression, accelerated also by GPUs, is used to extract the predictive capacity from the reservoir states. The results suggest that edge-of-chaos dynamics correspond to enhanced memory and prediction accuracy, supporting the potential of TVB-based reservoirs for brain-inspired machine learning.

Keywords: Reservoir computing \cdot The Virtual Brain \cdot Information based metrics.

1 Introduction

Reservoir computing (RC) [?,?] is a type of recurrent neural network architecture that uses a "reservoir" of interconnected, recurrent, and non-linear nodes to process sequential or temporal data. The reservoir projects input data into a high-dimensional state space. A readout layer then maps this space to the desired output. This process leverages the fading memory property, which allows the model to capture and temporarily store information with decaying characteristics [?]. From a biological standpoint, RC provides an interpretation of computation in neocortical microcircuits [?]. The superior cognitive achievements of higher vertebrate brains, such as conscious processing, may result from the comprehensive utilization of this adaptable neural circuit [19].

An optimal operating regime or a critical point of complexity may support neural computation, and self-organized criticality (SOC) is a competitive model for elucidating neural mechanisms [?,?,?,21,4]. SOC and complexity can be quantified using various metrics, such as the Perturbational Complexity Index (PCI), Detrended Fluctuation Analysis (DFA) to evaluate long-range temporal correlations, and the Lyapunov exponent (LYA) to estimate the rate of divergence or convergence of neural dynamics. Criticality is marked by the coexistence of maximal complexity or information richness (PCI) and power-law scaling or long-range temporal correlations, allowing for optimal information processing and adaptability in the brain [21,?,2].

It remains unknown how complexity affects the performance of simulated biological networks in predicting non-linear dynamics, a crucial aspect of understanding complex biological systems. Here, we address this issue by investigating the influence of complexity on the performance of these networks, with a focus on their ability to predict non-linear dynamics. To investigate the differences in optimal performance underlying active and resting states, two distinct brain models are implemented, acting as nodes of the reservoir network. Results show that these models exhibit distinct optimal performance regimes. One model excels in active states with high complexity, strong long-range correlations, and low chaos, while the other model performs optimally in resting states with high complexity, weak correlations, and high chaos.

2 Materials and Methods

RateML's [?,?,?] High Performance Computing (HPC) version of The Virtual Brain [18] (TVB) simulator is utilized to set up a grid of mean-field models, which provides for vast parallelization of the model's parametrization on multiple Graphics Processing Units (GPU). The process involves four key steps: injecting dynamics, training with ridge regression, running a simulation with the acquired weights, and prediction. To examine the reservoir's learning capacity, it is trained to predict the Lorenz dynamics [12], described by the following equations:

$$\frac{dx}{dt} = \sigma(y - x), \ \frac{dy}{dt} = x(\rho - z) - y, \ \frac{dz}{dt} = xy - \beta z. \tag{1}$$

The dynamics are injected into the TVB network. A neuro-realistic connectome of 96 nodes, serving as the interconnect for the TVB simulation, is utilized [?]. Nodes 10, 17, and 30 are selected as dedicated input nodes for this task, which are anatomically part of the frontal lobe and orbitofrontal cortex, situated close to the eyes (lateral orbitofrontal, pars orbitalis, and frontal pole). Nodes 15, 20, and 22 are selected as dedicated output nodes and form the layer that is trained to represent the desired dynamic, and are chosen from regions closest and most likely connected to the motor cortex (precentral, paracentral, and postcentral).

The learning phase runs for 625 time-steps, including a 125-time-step initialization phase, to stabilize the reservoir's dynamics and determine the weights. A teacher signal is used to train the reservoir to predict future states. During the training phase, the output nodes are fed with a teacher signal, which is a temporally advanced copy of the input signal. This means that the teacher signal provides the reservoir with a preview of the next state, allowing it to learn the temporal relationships between the current and next states.

Tikhonov Ridge regression [6] is employed to capture the system's dynamics and compute the weights necessary for prediction. After the new weights are acquired, a second simulation is initialized implementing these weights. This simulation is spun up for 375 steps using the Lorenz dynamics with different initial conditions. The resulting reservoir state is used to make an overall or macro prediction over 250 time-steps. The described method is similar to work from Tolle et al. [22]. The macro prediction is made after the second TVB simulation and reflects the overall quality of the fully trained reservoir.

In contrast to the macro prediction, micro predictions are made to enhance the dynamics during the second TVB simulation. These micro predictions are made with shorter intermediate simulation results, as shown in fig. 1.

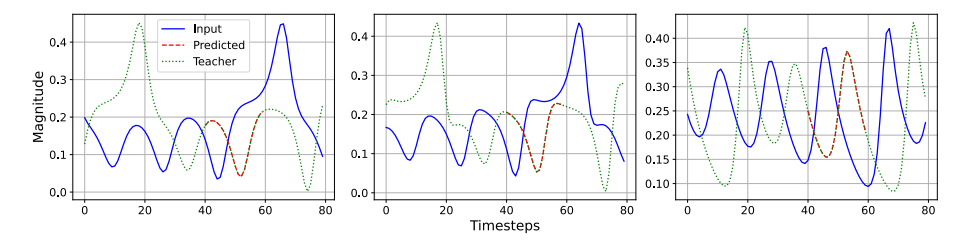


Fig. 1. Partial prediction for a position of the reservoir. The prediction (red) follows if the reservoir is in the state at the position 40 to 60 of the reservoir (blue). The teacher signal (green) is a temporally advanced copy the input signal and is used to create the temporal relation of the regression fit.

These intermediate micro predictions are then injected back into the second TVB simulation amplifying the current dynamics. The partial prediction is of the size of the trainer-teacher-delay, meaning that the next injection coincides with the correct phase of the reservoir. The resulting prediction is upsampled

to match the time basis on the GPU using spline interpolation. After obtaining the macro predictions, the mean squared error (MSE) with the true signal is calculated. The computations use a normalized mean squared error metric with an exponential decay weighting.

2.1 Mean-field neural mass models

The Montbrió-Pazó-Roxin (MPR) model [13] uses the Ott-Antonsen reduction [15] to describe the dynamics of an infinite ensemble of all-to-all coupled quadratic integrate-and-fire (QIF) neurons. The model has two state variables, r and V, representing the firing rate and average membrane potential of the QIF neurons. The Lorentz dynamics are injected on the first state variable, r.

The MPR model can exhibit synchronized and desynchronized states of activity, corresponding to resting and active states of brain activity [13]. The resting state is characterized by spontaneous fluctuations in neural activity, with moderate noise contributing to low-frequency fluctuations and irregular neural firing [4]. The active state corresponds to brain activity elicited in response to performing a specific cognitive or motor task. The model's parameters, including the synaptic weight J, feedback scaling parameter η , and external current I, can be adjusted to create an effective excitatory-inhibitory dynamic and simulate adaptation-like behavior [13]. The parameter η determines the strength of the self-feedback loop, while J controls the strength of the synaptic inputs. The external current I represents the level of external input applied to each neuron, with higher values corresponding to activity observed during cognitive tasks.

The Larter-Breakspear (LB) model [9] simulates the collective dynamics of excitatory and inhibitory populations within a cortical column, building upon classical Wilson-Cowan models [24]. The model incorporates nonlinear synaptic interactions, NMDA receptor dynamics, and intrinsic noise, enabling the study of complex brain activity patterns and criticality. The LB model's three state variables are V (mean membrane potential of excitatory pyramidal neurons), W (average number of open potassium ion channels) and Z (mean membrane potential of inhibitory interneurons) [5]. The Lorentz dynamics will be injected on the first state variable, V. The model can be tuned to simulate active and resting state brain dynamics by modulating the excitatory-to-excitatory synaptic strength ($a_{\rm ee}$), the mean threshold potential for excitatory neurons ($V_{\rm T}$), and ratio of NMDA to AMPA receptors ($r_{\rm nmda}$). Decreasing $a_{\rm ee}$ or increasing ($V_{\rm T}$) can lead to a decrease in the model's sensitivity to external inputs, simulating a more inactive state. Adjusting $r_{\rm nmda}$ can modulate the model's synaptic plasticity, allowing it to exhibit more stable, inactive-like dynamics.

2.2 Neural complexity

In the context of the brain, complexity refers to the intricate and dynamic organization of neural networks, encompassing the structure, function, and interactions of neurons and synapses. We select three measures to study the dynamics

Symbol	Description	Resting State	Active State
	Montbrió-Pazó-Roxin		
I	External Current	-0.5 to 0.0	2.0 to 4.0
J	Mean Synaptic Weight	12 to 14	15 to 16
η	Feedback Scaling	-4.6	-3.5 to -4.0
	Larter-Breakspear		
a_{ee}	Excitatory-to-excitatory synaptic strength	0.01	0.5
V_T	Threshold potential excitatory neurons	-30	-60mV
r_{nmda}	Ratio of NMDA to AMPA receptors	0.1	1.5

Table 1. Parameter settings for resting and cognitive task states in the MPR and Breakspear TVB models

of learning systems and represent the brain's complexity and criticality, as described in the following.

Perturbational Complexity Index (PCI) The PCI, a clinical metric for discriminating levels of consciousness, assesses differentiation and integration within brain networks [2,3,1]. It quantifies the complexity of averaged evoked Electroencephalogram (EEG) signals by targeting the spatiotemporal differentiation of deterministic and causal components [2]. The PCI is derived using the Lempel-Ziv complexity (LZc), which estimates Kolmogorov complexity and assesses the diversity of patterns within a signal [23,10]. The PCI is calculated as the ratio between the LZc and the source entropy H [2]:

$$PCI(s) = LZ(s)/H(s)$$
 (2)

A low PCI indicates reduced interaction between cortical areas, while a high PCI is observed when the initial perturbation propagates to a broad array of integrated areas, each responding distinctively [2]. The moment of perturbation is set to the moment of injection of the Lorentz dynamics into the reservoir.

The module from [3] has been used to implement the PCI on the GPU. The GPU-kernel parallelizes the computation of PCI for each unique TVB simulation, resulting in significant speedup compared to a serial implementation. The CUDA kernel calculates the PCI for a set of trials and sources using binarized data. The kernel includes: signal pre-processing, binarization, sorting, complexity computation, and normalization. Pre-processing involves performing centering, standardization, and binarization based on a given percentile threshold. The binary matrix is then sorted by rows based on the sum of elements in each row, prioritizing sources contributing more significantly to the signal. The LZc of the sorted binary matrix is computed converting binary rows into sequences of bits and identifying recurring patterns. After, the entropy of the binary matrix for normalization based on probabilities (p_1) and (p_0) is determined. The PCI was normalized using Lempel–Ziv complexity divided by signal entropy, improving reproducibility by reducing sensitivity to amplitude for instance. The results of the PCI are plotted in fig. 2 for MBR and in fig. 3 for LB.

Detrended Fluctuation Analysis Fractal dimensions are valuable tools for quantifying the complexity and self-similarity in neural systems [11]. In neuroscience, Detrended Fluctuation Analysis (DFA) has been applied to determine fractal dimension and study the temporal dynamics of neural signals [8]. DFA involves several steps to analyze the correlation properties of a time-series, including removing local trends, calculating the root-mean-square (RMS) fluctuations, and determining the scaling exponent (α) through a power-law relationship. The α value, also known as the Hurst exponent, measures the auto-correlation structure of a time series and ranges between 0 and 1 [7,8]. A Hurst exponent greater than 0.5 suggests persistent correlations, while a value less than 0.5 indicates anti-persistent correlations. The DFA is commonly expressed by the following formula [16]:

$$F(n) = \sqrt{\frac{1}{N} \sum_{i=1}^{N} [y(i) - y_{\text{fit}}(i)]^2}$$
 (3)

Where F(n) is the RMS fluctuation for box size n, N is the total number of data points, y(i) is the time series data at point i, $y_{\rm fit}(i)$ is the best-fit polynomial within a specific window at point. The scaling exponent α is determined by analyzing the relationship between F(n) and the box size n through a power-law relationship: $F(n) \propto n^{\alpha}$. The final output, the scaling exponent (α) , provides insight into the fractal properties of the data, indicating whether the time series is more random or correlated in nature.

The Nolds [17] Python library, which includes the DFA, is used as a basis to implement this algorithm on the GPU. The GPU kernel implements two-dimensional parallelism for each unique TVB simulation and its regions. Each thread processes one simulation-region pair, dividing the data into non-overlapping windows and calculating the RMS fluctuations. The kernel computes the logarithm of both the fluctuation and the window size, using these values to calculate the scaling exponent (α) , which characterizes the complexity of the time series. The results of the DFA are plotted in fig. 2 for MBR and in fig. 3 for LB. DFA exponents were estimated via linear regression on log-log fluctuation vs. window size and reported per region without further normalization, as the exponent is inherently dimensionless and amplitude-independent.

Chaoticity The largest Lyapunov exponent (LYA) is used to quantify the intrinsic chaoticity of a system, denoting the rate at which initially similar trajectories in the system's phase space diverge [14,20]. A positive LYA indicates chaotic behavior, while a negative exponent suggests periodic or stable behavior [14]. The magnitude of the LYA correlates with the degree of chaos in the system [20]. The Python library Nolds [17] is used to implement the LYA on the GPU and is expressed by the following formula:

$$\lambda = \lim_{t \to \infty} \frac{1}{t} \sum_{i=0}^{t-1} \ln \left| \frac{d}{dx} f(x_i) \right| \tag{4}$$

Where x_i is the delay vector at time $i, f(x_i)$ is the mapping of x_i to the next point in the trajectory, as part of the time-delay embedding process.

The GPU kernel implements two-dimensional parallelism for each unique TVB simulation and its regions. It uses time-delay embedding to transform the input time series into a high-dimensional space, capturing the system's dynamics. The resulting matrix stores the estimated LYA for each region in each simulation. The results of the LYA are plotted in fig. 2 for MBR and in fig. 3 for LB.

3 Results

3.1 Parameters Space Exploration

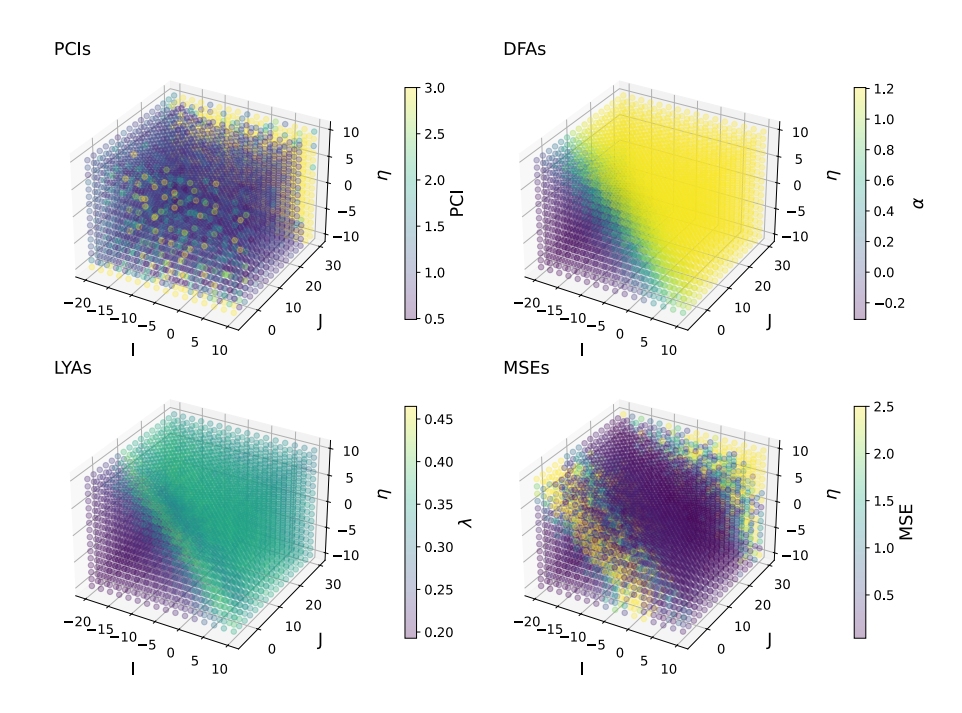


Fig. 2. Complexity (PCIs), fractality (DFAs), chaoticity (LYAs) and mean squared error of the fit (MSEs) for the Montbrió-Pazó-Roxin model as functions of the external current (I), mean synaptic weight (J) and the feedback scaling (η) .

For the Montbrió-Pazó-Roxin model, the results of sweeping the external current I, feedback scaling η , and mean synaptic feedback J parameters while learning to predict the Lorentz dynamics (??) are shown in fig. 2. A clear separation between lower and upper tetrahedrons is observed for the DFA and LYA metrics and MSE. The plane separates the higher DFA values from the lower LYA values.

A near critical regime is characterized by lower values of LYA and persistent correlations by higher than .5 values for DFA. Thus, optimal learning conditions seem to appear around the separation, where also an area of lower MSE values is found.

Overall, the system remains in a chaotic regime $(\lambda>0)$ but within a controlled range (0.2-0.5), indicating persistent sensitivity to initial conditions without extreme chaos. A DFA exponent greater than 0.5 suggests strong long-range correlations, indicating persistent memory, whereas a DFA exponent less than 0.5 indicates anti-persistent behavior, characterized by a fast decay of correlations. The PCI exhibits a more scattered distribution, with high values appearing throughout the parameter space. This suggests that complexity is a localized phenomenon, rather than a global trend. Notably, the results indicate that complexity is not solely tied to chaotic behavior or long memory, revealing a more nuanced relationship between these concepts.

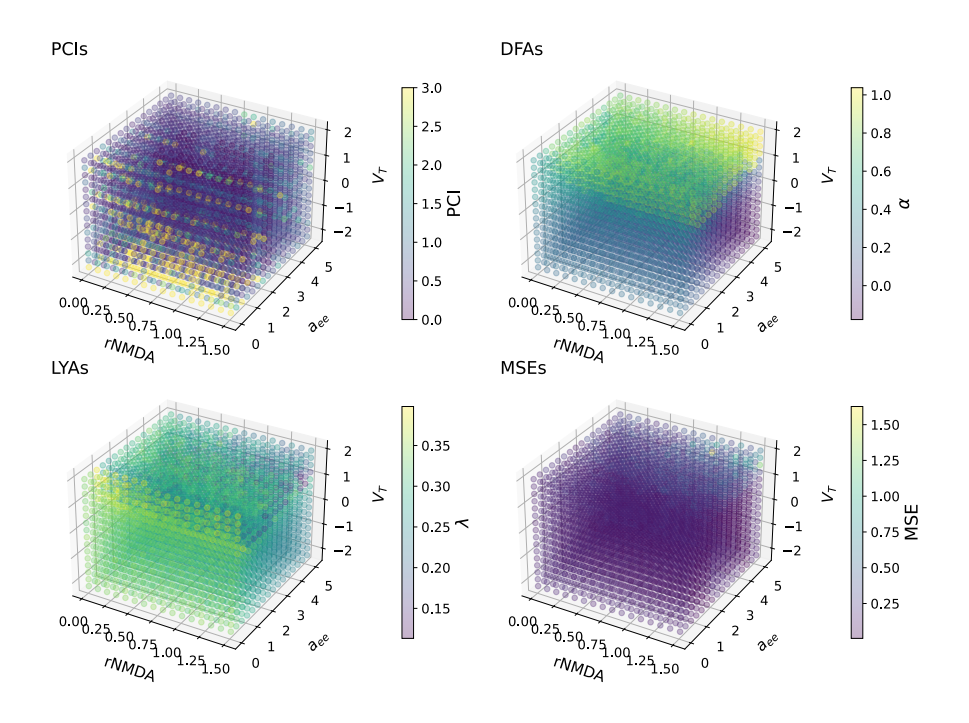


Fig. 3. Complexity (PCIs), fractality (DFAs), chaoticity (LYAs) and mean squared error of the fit (MSEs) for the Larter-Breakspear model as functions of the excitatory-to-excitatory synaptic strength (a_{ee}) , the mean threshold potential for excitatory neurons (V_T) , and the ratio of NMDA to AMPA receptors (r_{nmda}) .

The analysis of the Larter-Breakspear model are shown in fig. 3 for a parameter sweep of the excitatory-to-excitatory synaptic strength (a_{ee}) , the mean

threshold potential for excitatory neurons (V_T) , and ratio of NMDA to AMPA receptors (r_{nmda}) is shown in fig. 3. The PCI is scattered, indicating a complex and nonlinear relationship between the model's parameters and its dynamics. A clear relationship is observed between the adaptation current parameter $V_{\rm T}$ and the DFA exponent, with higher $V_{\rm T}$ values corresponding to higher DFA values, which vary from 0.0 to 1.0. Similarly, higher $V_{\rm T}$ values are associated with lower LYA, which range from 0.15 to 0.35. The analysis of the MSE reveals that it is overall low, indicating that it captures the underlying dynamics of the system reasonably well. However, an interesting observation is that the MSE starts to rise when LYA is low and DFA exponent is high, when $V_{\rm T}$ is higher and $a_{\rm ee}$ is at its maximum. Just before the rise in MSE, there is a small area where high DFA and low LYA overlap. A higher threshold voltage $V_{\rm T}$ likely increases neuron excitability, making dynamics more stable. Higher a_{ee} (excitatory-excitatory strength) could drive strong recurrent excitation, leading to an overly stable regime. This suggests a narrow transition where the system has strong memory (DFA high) but is still near marginal stability (low LYA), possibly close to a critical-like regime before becoming too stable.

3.2 Information Distribution

The distributions of MSE for active and resting states are shown in the left panels (A, C) of fig. 4, and are based on predefined parameter masks. The right panels (B, D) show the distributions of the MSE based on different metric masks, categorizing simulations into high and low values of PCI, DFA, and LYA. The parameter masks are based on the subset of parameters defined in ?? to identify the predefined regions of the MSE space that coincide with the active or resting state of the model. The metrics masks are a combination of high/low PCI, DFA and LYA as shown in the legend of fig. 4. The threshold values for the PCI (≈ 1.0) and LYA (≈ 0.3) are based on the median of its values and the DFA (0.5) is based on the aforementioned value from literature.

The distribution of MSE values in fig. 4 reveals that the MBR model achieves its best fits more frequently when in an active state (A). In contrast, the LB model performs optimally when in a resting state (C). Furthermore, the metrics-based masks indicate that the MBR model prefers lower complexity for its best fits, when DFA is higher, indicating strong long-range correlations and LYA is lower, indicating operation at criticality (B), whereas the LB model favors higher complexity, when DFA is lower and LYA is higher (D), indicating less correlated fluctuations and more pronounced chaotic dynamics. This disparity likely arises from the distinct intrinsic dynamical properties of the two models, with the MBR model suited to active states with sustained, self-organized neural activity, and the LB model favoring resting states with spontaneous fluctuations and higher unpredictability.

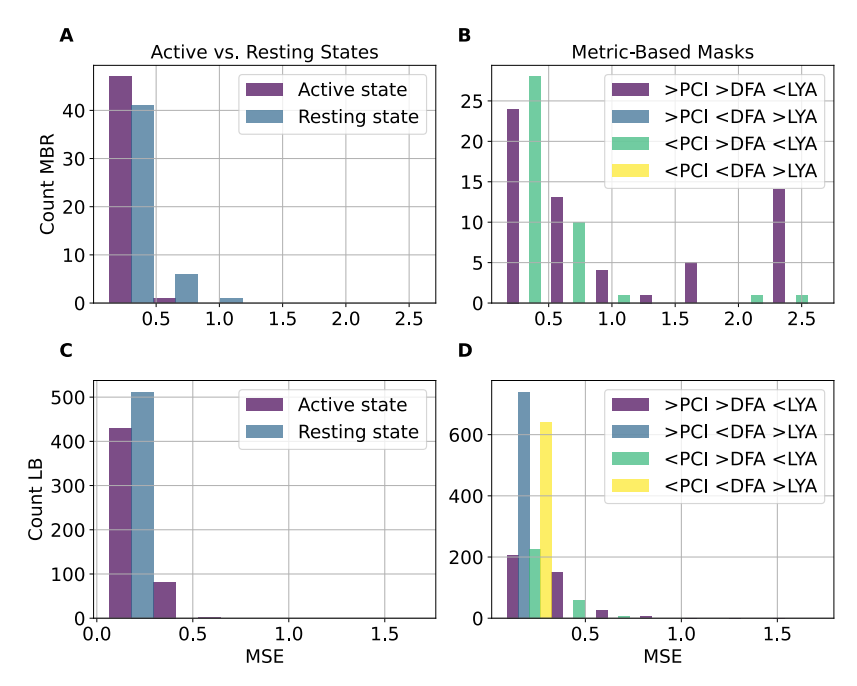


Fig. 4. Distribution of the Mean Squared Error fitting the predicted Lorentz Dynamics for the Montbrió-Pazó-Roxin (A,B) and the Larter-Breakspear model (C,D). The distributions are based on predefined (A, C) parameter and metrics-based (B, D) masks.

4 Conclusion/Discussion

The reservoir computer framework implemented in TVB offers a powerful tool for exploring learning dynamics in complex systems. By considering TVB's interconnected nodes as the elements of a reservoir, reservoir learning is intersected with brain simulation and analysis. Making use of metrics like Lyapunov exponents, Detrended Fluctuation Analysis, and the Perturbational Complexity Index, different dynamical regimes can be characterized and the effect of these metrics on machine learning systems can be studied. The framework is available at https://github.com/DeLaVlag/TVB-Reservoir.

The two brain models exhibit distinct behaviors in terms of their optimal performance regimes. The MBR model achieves its best fits when in an active state, characterized by high complexity, strong long-range correlations, and low chaos, whereas the LB model achieves this in a resting state, marked by high complexity, weak long-range correlations, and high chaos. Interestingly, the MBR model prefers lower complexity for its best fits, when DFA is higher, indicating strong long-range correlations and LYA is lower, indicating operation at criticality. Whereas the LB model favors higher complexity, when DFA is lower and LYA is higher, indicating less correlated fluctuations and more pronounced chaotic dynamics.

Acknowledgments. We thank Wouter Klijn, Jennifer S. Goldman, Giulia De Bonis, Pier Stanislao Paolucci and Cosimo Lupo for their significant contributions to the discussion on TVB-Reservoir's architecture, implementation, and metrics. Their expertise and feedback have been invaluable in shaping this paper, and we appreciate their time and collaboration. The research leading to these results has received funding from the European Union's Horizon 2020 Framework Program for Research and Innovation under the Grant Agreement 101058516 (eBRAIN-Health). This research was also supported by the Helmholtz Joint Lab "Supercomputing and Modeling for the Human Brain". Open Access publication was funded by the Deutsche Forschungsgemeinschaft (DFG, German Research Foundation)—491111487.

Disclosure of Interests. The authors declare no conflicts of interest.

References

- Arsiwalla, X.D., Verschure, P.: Measuring the complexity of consciousness. Front. Neurosci. 12(JUN), 1-6 (2018). https://doi.org/10.3389/fnins.2018.00424
- Casali, A.G.e.a.: A theoretically based index of consciousness independent of sensory processing and behavior. Science Translational Medicine 5(198) (2013). https://doi.org/10.1126/scitranslmed.3006294
- Casarotto, S.e.a.: Stratification of unresponsive patients by an independently validated index of brain complexity. Ann Neurol 80(5), 718–729 (Nov 2016). https://doi.org/10.1002/ana.24779
- 4. Deco, G.e.a.: Emerging concepts for the dynamical organization of resting-state activity in the brain. Nature Reviews Neuroscience **12**(1), 43–56 (2011)
- Gaglioti, G., Nieus, T.R., Massimini, M., Sarasso, S.: Investigating the Impact of Local Manipulations on Spontaneous and Evoked Brain Complexity Indices: A Large-Scale Computational Model. Applied Sciences (Switzerland) 14(2) (2024). https://doi.org/10.3390/app14020890
- 6. Hoerl, A.E., Kennard, R.W.: Ridge regression: Biased estimation for nonorthogonal problems. Technometrics **12**(1), 55–67 (1970)
- 7. Hurst, H.E.: Long-term storage capacity of reservoirs. Transactions of the American Society of Civil Engineers 116, 770–799 (1951)
- 8. Ihlen, E.A.: Introduction to multifractal detrended fluctuation analysis in matlab. Frontiers in Physiology 3 (2012). https://doi.org/10.3389/fphys.2012.00141
- 9. Larter, e.a.: A coupled ordinary differential equation lattice model for the simulation of epileptic seizures. Chaos 9(3), 795 (1999)
- Lempel, A., Ziv, J.: On the complexity of finite sequences. IEEE Transactions on Information Theory 22(1), 75–81 (1976)
- Linkenkaer-Hansen, K.e.a.: Long-range temporal correlations and scaling behavior in human brain oscillations. The Journal of neuroscience 21(4), 1370–1377 (2001). https://doi.org/10.1523/JNEUROSCI.21-04-01370.2001
- 12. Lorenz, E.N.: Deterministic non-periodic flow. Journal of the Atmospheric Sciences **20**(2), 130–141 (1963)
- Montbrió, E., Pazó, D., Roxin, A.: Macroscopic description for networks of spiking neurons. Physical Review X 5(2), 1-15 (2015). https://doi.org/10.1103/PhysRevX.5.021028
- 14. Ott, E.: Chaos in Dynamical Systems. Cambridge University Press (1993)
- Ott, E., Antonsen, T.M.: Low dimensional behavior of large systems of globally coupled oscillators. Chaos (Woodbury, N.Y.) 18(3), 37113 (sep 2008). https://doi.org/10.1063/1.2930766

- Peng, C.K.e.a.: Mosaic organization of dna nucleotides. Physical Review E 49(2), 1685 (1995)
- 17. Santos, M.C.: nolds: A python library for nonlinear time series analysis (2017). https://doi.org/10.5281/zenodo.1038497
- Sanzleon, P.e.a.: The virtual brain: A simulator of primate brain network dynamics. Front. Neuroinform. 7(MAY) (2013). https://doi.org/10.3389/fninf.2013. 00010
- Seoane, L.F.: Evolutionary aspects of reservoir computing. Philosophical Transactions of the Royal Society B: Biological Sciences 374(1774) (2019). https://doi.org/10.1098/RSTB.2018.0377
- Strogatz, S.H.: Nonlinear Dynamics and Chaos: With Applications to Physics, Biology, Chemistry, and Engineering. Westview Press (2014)
- Toker, D.e.a.: Consciousness is supported by near-critical slow cortical electrodynamics. Proceedings of the National Academy of Sciences of the United States of America 119(7), 1–12 (2022). https://doi.org/10.1073/pnas.2024455119
- 22. Tolle, H.M., Luppi, A.I., Seth, A.K., Mediano, P.A.M.: Evolving reservoir computers reveals bidirectional coupling between predictive power and emergent dynamics (2024), http://arxiv.org/abs/2406.19201
- 23. Vitanyi, P.M., Li, M.: An Introduction to Kolmogorov Complexity and its Applications, vol. 34. Springer Heidelberg (1997)
- 24. Wilson, H.R., Cowan, J.D.: Excitatory and inhibitory interactions in localized populations of model neurons. Biophysical Journal **12**(1), 1–24 (1972)